Immobilizing Gold Nanoparticles in Mesoporous Silica Covered Reduced Graphene Oxide: A Hybrid Material for Cancer Cell Detection through Hydrogen Peroxide Sensing

Swarup Kumar Maji,[†] Sivaramapanicker Sreejith,[†] Amal Kumar Mandal,[†] Xing Ma,[†] and Yanli Zhao*,[†,‡]

[†]Division of Chemistry and Biological Chemistry, School of Physical and Mathematical Sciences, Nanyang Technological University, 21 Nanyang Link, Singapore 637371, Singapore

[‡]School of Materials Science and Engineering, Nanyang Technological University, 50 Nanyang Avenue, Singapore 639798, Singapore

S Supporting Information

ABSTRACT: A new kind of two-dimensional (2-D) hybrid material (RGO-PMS@AuNPs), fabricated by the immobilization of ultrasmall gold nanoparticles (AuNPs, ~3 nm) onto sandwich-like periodic mesopourous silica (PMS) coated reduced graphene oxide (RGO), was employed for both electrocatalytic application and cancer cell detection. The hybrid-based electrode sensor showed attractive electrochemical performance for sensitive and selective nonenzymatic detection of hydrogen peroxide (H_2O_2) in 0.1 M phosphate buffered saline, with wide linear detection range (0.5 μM to 50 mM), low detection limit (60 nM), and good sensitivity (39.2 μA mM^{-1} cm^{-2}), and without any interference by common interfering agents. In addition, the sensor exhibited a high capability for glucose sensing and H_2O_2 detection in human urine. More interestingly, the hybrid was found to be nontoxic, and the electrode sensor could sensitively detect a trace amount of H_2O_2 in a nanomolar level released from living tumor cells (HeLa and HepG2). Because the hybrid presents significant properties for the detection of bioactive species and certain cancerous cells by the synergistic effect from RGO, PMS, and AuNPs, it could be able to serve as a versatile platform for biosensing, bioanalysis, and biomedical applications.

KEYWORDS: biosensing, cancer detection, gold nanoparticles, periodic mesoporous silica, reduced graphene oxide
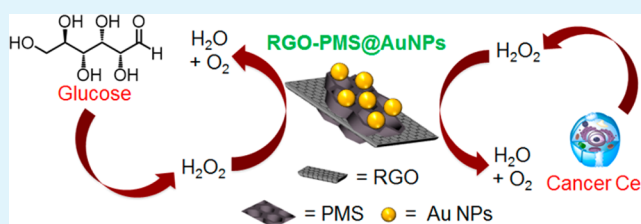
1. INTRODUCTION

The fabrication of a suitable quantitative assay for rapid and accurate determination of hydrogen peroxide (H_2O_2) in biological systems is of practical importance in biology, biomedicine, food security, and environmental protection.[1−3] H_2O_2 is the byproduct of a wide range of biological and chemical processes and also generated by incomplete reduction of oxygen.[4] Because of strong oxidizing and reducing properties, it has been widely used in food, pharmaceutical, biomedical, paper, and chemical industries.[5] In living systems, H_2O_2 is produced by most oxidases in mitochondria and can reach various cellular compartments by diffusing out through the membranes.[6] It is also noteworthy that H_2O_2 can generate reactive oxygen species (ROS), excess of which can lead to different kinds of disorders in the body, such as Parkinson's, Alzheimer's, atherosclerosis, heart attack, and cancer.[7,8] In contrast, emerging evidence identifies that an appropriate level of H_2O_2 and ROS plays significant roles in the function and signal transduction of cells.[9,10] Because H_2O_2 is the byproduct of many enzymatic reactions, its concentration can also be used as an indicator for tracing the progress of biochemical reactions.

During the past few years, several measurement techniques for the detection of H_2O_2 have been explored, including spectrometry,[11] fluorometry,[12] chromatography,[13] cell imaging,[14] and electrochemical methods.[15,16] Among them, the electrochemical technique has proven its application potential due to its advantages of simple instrumentation, easy miniaturization, good quantitative determination, high sensitivity and selectivity, as well as rapid response time. The electrochemical technique using electrode devices fabricated based on catalytic reduction of H_2O_2 by a natural enzyme, horseradish peroxidase (HRP), was found to be an attractive method.[17] However, its serious disadvantages have largely limited its practical applications.[18] A solution was proposed using nonenzymatic artificial biosensors. In particular, precious metal nanoparticles,[19,20] carbon nanomaterials,[21,22] and metal oxide/sulfide semiconductors[23,24] have been widely employed due to their unique electronic and catalytic properties to enhance catalytic activity, high surface to volume ratio, suitable biocompatibility, low cost preparation, and good stability. Among various nanoparticles, gold nanoparticles (AuNPs) provide an appropriate platform for the immobilization of biomolecules to retain their biological activity and to facilitate the electron transfer between the immobilized biomolecules

Scheme 1. Schematic Representation for the Synthesis of RGO-PMS@AuNPs
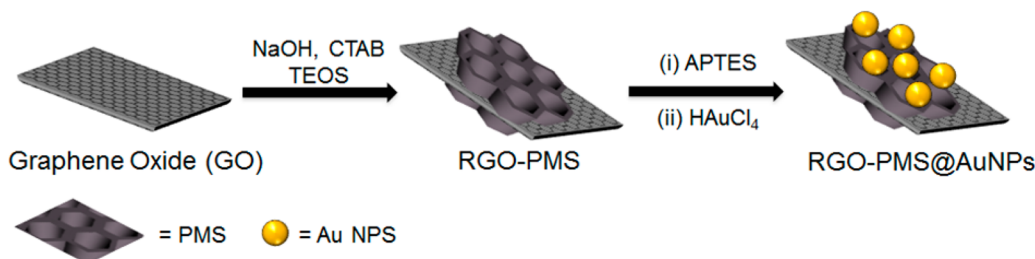
and electrode substrates, leading to enhanced analytical performance as compared to other biosensors.[25] Moreover, Au and its alloy have shown attractive catalytic performance for H_2O_2 determination with a very low detection limit of 2 μM.[26] Despite the enhanced activity and sensitivity, biosensors made from single-component nanoparticles are still not sensitive enough for detecting H_2O_2 produced by cellular activities at nanomolar concentrations.[27]

On the other hand, two-dimensional (2-D) graphene sheet has attracted significant attention[28] in synthesizing the nanohybrids for the fabrications of various electrical devices,[29] drug delivery carriers, and bioimaging systems.[30,31] A lot of effort has been made for the construction of graphene/AuNP hybrid materials for various applications ranging from electronic devices[32,33] to biosensors for effective detection of small molecules.[34−40] To the best of our knowledge, however, study to use the 2-D nanohybrid of AuNP-encapsulated sandwich-like periodic mesopourous silica (PMS) coated reduced graphene oxide (RGO) for the fabrication of electrochemical sensors toward sensitive detection of H_2O_2 has not been reported so far. Herein, we developed a facile and robust synthetic approach to prepare a new generation 2-D nanohybrid system of well-dispersed AuNPs over PMS coated RGO (RGO-PMS@AuNPs), which could act as an excellent platform for highly sensitive and selective detection of H_2O_2 at a nanomolar concentration level. Although PMS is non-conductive in nature, it has been reported that, when a hybrid is formed by sandwich-like coating of PMS on RGO, it has the ability to show semiconductor-like behavior.[41] By using RGO-PMS@AuNPs-based electrode sensor, the H_2O_2 level in human urine and glucose could also be detected with an enhanced sensitivity on account of the synergistic effect from RGO, PMS, and AuNPs. Because the electrochemical sensitivity of the sensor device could reach as low as 60 nM, it was successfully utilized to detect H_2O_2 liberated from cancer cells.

2. EXPERIMENTAL SECTION

2.1. Synthesis of RGO-PMS. Graphene oxide (GO) was synthesized according to a literature report,[42] and RGO-PMS was prepared by a modified method based on a previous report.[41] Briefly, a dilute aqueous suspension of GO was prepared by mixing a GO suspension (1 mg mL^{-1}, 5 mL) with water (120 mL). Next, NaOH aqueous solution (0.5 mL, 2 M) was added to the suspension, which was heated to 80 °C under sonication for 20 min. Cetyltrimethy-lammonium bromide (CTAB, 4 mg) in water (50 mL) was added into the above suspension with vigorous stirring for another 30 min. After the suspension was cooled to room temperature, tetraethyl orthosilicate (TEOS, 4 mL) was added. The solution mixture was stirred for 4 h. The obtained material was washed with HCl/MeOH (1:1) four times followed by ethanol two times. RGO-PMS was finally collected by centrifugation.

The surface modification from −OH to −NH$_2$ on RGO-PMS was carried out by the introduction of 3-aminopropyl triethoxysilane

(APTES). RGO-PMS (100 mg) in ethanol (100 mL) in a round-bottom flask was mixed with APTES (200 μL) under continuous stirring. The mixture was refluxed at 80 °C for 12 h and then cooled to room temperature naturally. The surface-modified material (RGO-PMS-NH$_2$) was collected by centrifugation and washed with ethanol.

2.2. Synthesis of RGO-PMS@AuNPs. RGO-PMS-NH$_2$ (10 mg) was dispersed in water (10 mL), and then HAuCl$_4$ aqueous solution (10 mM, 1 mL) was added to the suspension. The reaction mixture was allowed to react for 6 h. After the reaction mixture was heated at 80 °C for 2 h, it was cooled to room temperature. The final product (RGO-PMS@AuNPs) was collected by centrifugation and washed with ethanol.

2.3. Electrochemical Measurements. Electrochemical measure-ments were carried out in a cell containing phosphate buffered saline (PBS, 10 mL, 0.1 M, pH 7.4) with a typical cell setup, in which platinum wire was used as auxiliary electrode, Ag/AgCl electrode as reference, and RGO-PMS@AuNPs modified glassy carbon (RGO-PMS@AuNPs/GC) as the working electrode. For the preparation of RGO-PMS@AuNPs/GC, RGO-PMS@AuNPs (1 mg) were dispersed in ethanol (40 μL), and then the colloidal suspension (10 μL) was dropped onto the GC electrode surface (3 mm). After being dried in air, Nafion solution (4 μL, 0.5%) was dropped onto the surface followed by dryness. Finally, the modified electrode was washed with distilled water and then dried. In the case of glucose sensing, glucose oxidase (GOD, 5 mg) was mixed with RGO-PMS@AuNPs (1 mg) in ethanol (40 μL) for the fabrication of RGO-PMS@AuNPs-GOD/GC electrode. To carry out the determination of H_2O_2 in human urine, freshly voided human urine sample was collected from a healthy volunteer, which was diluted with 0.1 M PBS (pH 7.4) and stored for 60 min. Electrochemical impedance spectroscopy (EIS) measurements were carried out in KCl (10 mL, 0.1 M) and Fe(CN)$_6$$^{4-/3-}$ (5 mM) mixture solution (1:1) under the frequency range from 0.1 Hz to 10.0 kHz using a similar electrode setup.

2.4. Cancer Cell Detection. HEK 293, HeLa, and HepG2 cells were seeded into three different 75 cm^2 flasks in DMEM (Dulbecco's Modified Eagle's Medium) cell culture medium containing 10% fetal bovine serum (FBS) and penicillin (1%), and grown under a humidified atmosphere with 5% CO$_2$ at 37 °C. After the growth of ∼90% confluence, the cells were collected by centrifugation and washed with PBS three times. The collected cells were separately suspended into PBS (10 mL, 0.1 M, pH 7.4, and 37 °C). Each mixture (10 mL) was then used as an electrolyte for the current response measurements using the same protocol for H_2O_2 detection. After reaching the steady-state current, PMA (phorbol 12-myristate 13-acetate, 0.3 μL, 1 μg mL^{-1}) was added, and the change in the current signal was monitored. For the catalase inhibition, catalase solution (20 μL, 340 000−1 360 000 unit mL^{-1}) was added into the PBS medium.

2.5. Characterizations. Powder X-ray diffraction (XRD) pattern was obtained by Shimadzu XRD-6000 with monochromatic Cu Kα radiation (λ = 1.540598 Å). Field emission scanning electron microscope (FESEM) image was taken using a JEOL JSM-6700F microscope with 5 kV accelerating voltage. Transmission electron microscopy (TEM) and high-resolution TEM (HRTEM) analyses were performed on a FEG-TEM (JEM-2100F, JEOL, Japan) operated at 200 kV. Zeta potential measurements were conducted using a MavernNanosizer instrument. X-ray photoelectron spectroscopy (XPS) was carried out via a SPECS HSA3500 plus spectrometer
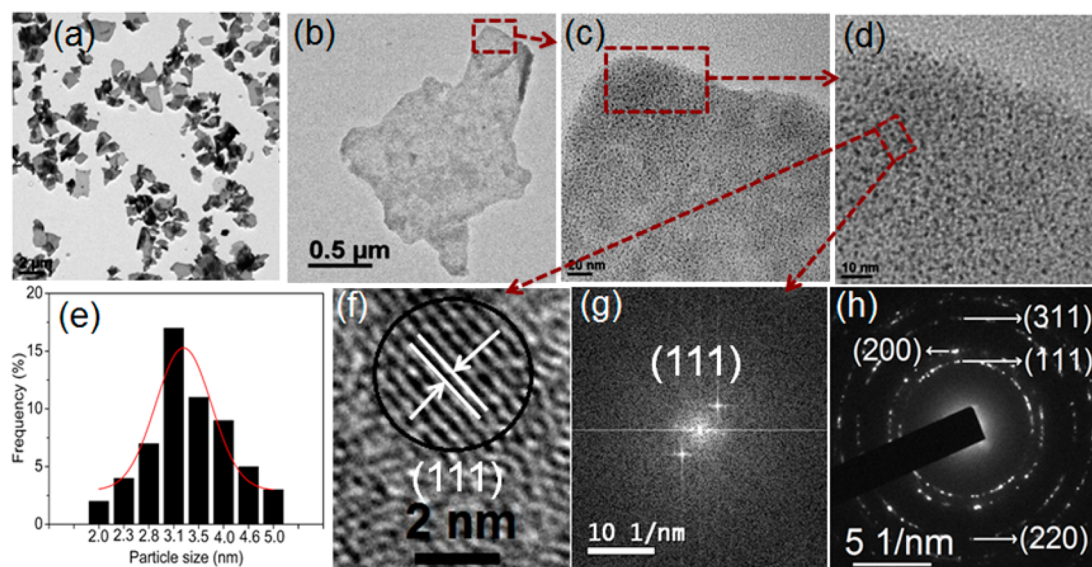
Figure 1. (a−d) A series of TEM and HRTEM images, (e) particle size distribution, (f) fringe pattern, (g) live FFT, and (h) SAED pattern of RGO-PMS@AuNPs.
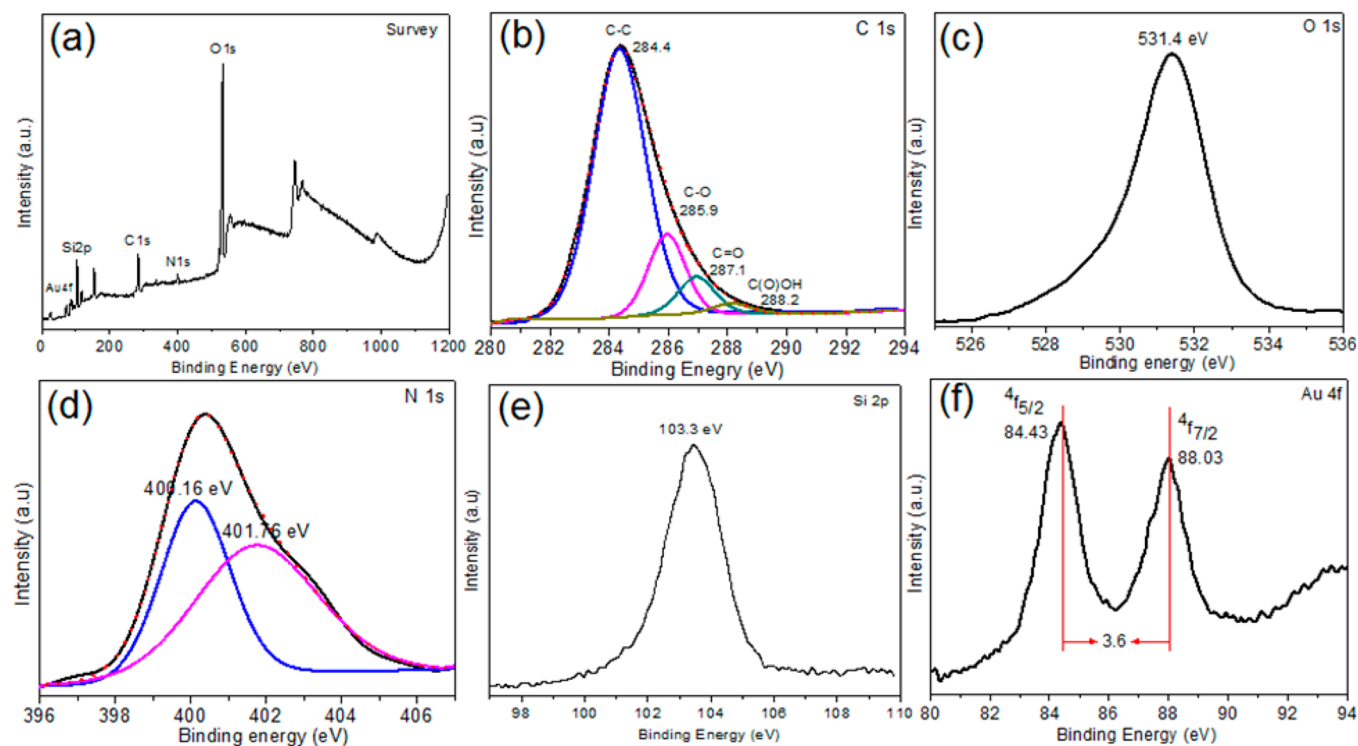

Figure 2. (a) XPS survey spectrum, (b) C 1s, (c) O 1s, (d) N 1s, (e) Si 2p, and (f) Au 4f spectra of RGO-PMS@AuNPs.

using Mg X-ray source. Raman spectra of the materials on cleaned copper substrates were measured with a Raman microscope (LabRAM HR, Horiba Yvon). The excitation wavelength of the irradiation light was 633 nm (He−Ne Laser, Melles Griot), and the signals were collected using a 100× objective lens. Brunauer−Emmett−Teller (BET) measurements were carried out using a Micromeritics ASAP 2020 M automated sorption analyzer. Fourier transform infrared spectroscopy (FTIR) was recorded on a JASCO FTIR-460 Plus spectrophotometer. Electronic absorption spectra were recorded on a Shimadzu UV-3101 spectrophotometer. Electrochemical experiments were carried out using a Gamry potentiostat/galvanostat (Reference 600).

3. RESULTS AND DISCUSSION

3.1. Material Synthesis and Characterization. 2-D hybrid material RGO-PMS@AuNPs were synthesized by immobilizing small AuNPs (∼3 nm) on sandwich-like PMS coated RGO (Scheme 1). First, PMS coated RGO (RGO-PMS) with vertically oriented mesopourous channels was prepared.[42] PMS covered on the surface of RGO could act as a stabilizing agent to prevent serious aggregation of individual RGO by weakening the π−π stacking interaction between RGO nanosheets.[43,44] Finally, the immobilization of small and well-dispersed AuNPs on the surface of RGO-PMS was conducted via an in situ reduction of $HAuCl_4$ as the precursor to yield the
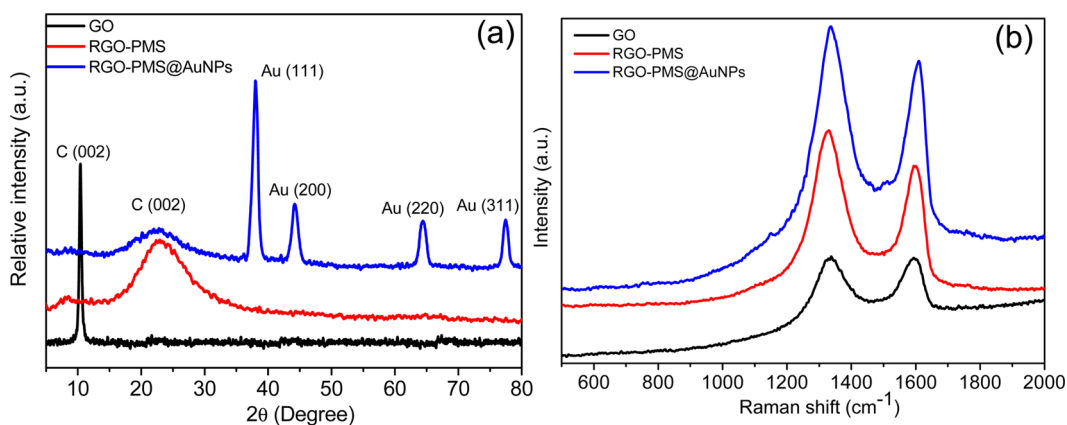
13650

dx.doi.org/10.1021/am503110s | ACS Appl. Mater. Interfaces 2014, 6, 13648−13656

Figure 3. (a) Wide-angle powder XRD patterns and (b) Raman spectra of GO, RGO-PMS, and RGO-PMS@AuNP.

RGO-PMS@AuNPs nanohybrid.[45] Before the reduction, −OH groups of PMS were converted to −NH$_2$ groups for the coordination with AuCl$_4^-$ through the lone pair electrons of nitrogen atoms to the metal atoms.

UV−vis, FTIR, and zeta potential (ζ) measurements (Figures S1 and S2 as well as related discussions in the Supporting Information) were carried out to characterize the hybrid materials. The structural and morphological characterization was performed by TEM and HRTEM. As shown in Supporting Information Figure S3, both sides of GO were coated with PMS to give sandwich-like 2-D RGO-PMS with a size range from 200 nm to 1 μm. The vertically oriented mesoporous channels were clearly observed in the HRTEM image of RGO-PMS (Supporting Information Figure S3c). The TEM and HRTEM images (Figure 1a−d) of the final hybrid RGO-PMS@AuNPs show the deposition of uniformly dispersed AuNPs with an average size of 3.1 nm over RGO-PMS (Figure 1e). The HRTEM image (Figure 1f) also exhibits well-crystalline lattice fringes of AuNPs in RGO-PMS@AuNPs with an interplanar distance of ∼0.235 nm, which can be assigned to the (111) plane of the face center cubic (f_{cc}) structure of Au. The single crystalline nature with a similar interplanar distance was also observed from live fast-Fourier transform (FFT) image (Figure 1g). The selected area electron diffraction (SAED) pattern (Figure 1h) exhibits four distinct concentric rings corresponding to the (111), (200), (220), and (311) planes of f_{cc} structure of Au (JEPDS no. 04 0784). The presence of distinct concentric rings also implies the well-crystalline nature of AuNPs.

XPS was then adopted (Figure 2), in which the survey spectrum and high-resolution spectra show the existence of C, O, N, Si, and Au elements in the corresponding regions for RGO-PMS@AuNPs. In the C 1s region (Figure 2b), it is interesting to note that the peak corresponding to the C−C skeleton at 284.4 eV is the major feature, whereas the intensities of the hydroxy, epoxy, and carbonyl groups at 285.9, 287.1, and 288.2 eV, respectively, are markedly reduced, demonstrating the significant restoration of the graphitic lattice. In the case of N 1s region (Figure 2d), the deconvoluted peaks at 400.16 and 401.76 eV originated from the presence of amine and nitro groups in the hybrid. In the high-resolution XPS spectrum of Au (Figure 2f), the Au 4f$_{7/2}$ and Au 4f$_{5/2}$ peaks locate at 88.03 and 84.43 eV, respectively, indicating the complete reduction of Au^{3+} on the RGO-PMS surface.[36] A small blue shift in the Au 4f spectrum was observed due to the

electron transfer within the hybrid, proving a strong interaction between AuNPs and RGO-PMS.[37]

Further structural characterizations were conducted by powder XRD and Raman spectral analyses. In the XRD pattern, the (002) plane at 10.4° for GO shifted to 23.5° (the (002) plane of RGO) after the PMS coating, indicating the formation of RGO (Figure 3a). The XRD pattern of the final hybrid also contains the (002) plane at 23.4° for RGO, along with 38.1°, 44.26°, 64.5°, and 77.52° peaks, which well match with the SAED pattern as well as the standard JCPDS data (04 0784) of f_{cc} Au corresponding to the (111), (200), (220), and (211) lattice planes. The crystallite diameter of AuNPs was calculated to be 2.8 nm using the Debye−Scherrer equation,[23] which is close to the value (3.1 nm) obtained from the TEM analysis. The Raman spectra of GO and RGO-PMS exhibit the presence of the D band at ∼1330 cm^{-1} corresponding to the defect induced breathing mode of A$_{1g}$ symmetry and the G band at ∼1590 cm^{-1} due to some degree of graphitization mode of E$_{2g}$ symmetry (Figure 3b). That the intensity ratio of I_D/I_G increased from 0.995 to 1.16 for GO to RGO-PMS further supports the formation of RGO. The Raman spectrum of the hybrid also shows the presence of D and G bands along with an obvious upshift of the G band for about 10 cm^{-1} after the deposition of AuNPs due to the electron−phonon coupling (Figure 3b).[37]

In the N$_2$ adsorption/desorption measurements, both RGO-PMS and RGO-PMS@AuNPs show typical type-IV isotherms with a distinct H2 hysteresis loop, indicating the mesoporous nature of the materials (Supporting Information Figure S4). The average pore size distribution curves reveal the narrow size distribution at ∼3.1 nm for both cases (inset of Supporting Information Figure S4). However, the BET surface area decreased from 862.37 to 542.34 m^2 g^{-1} after the deposition of AuNPs on RGO-PMS. Because the mean pore size of the silica layer was about 3.1 nm and the average diameter of AuNPs is around 3 nm, it could be suggested that AuNPs not only distribute on the PMS, but also locate inside the pores, which are reflected by the reduced BET surface area. The observed BET surface area and pore size of the hybrid are large enough for providing sufficient interface between the analyte and the substrate.

3.2. Electrochemical Sensing of Hydrogen Peroxide. The developed 2-D nanohybrid was then employed as an electrode material to fabricate a sensor device for electrochemical detection of H$_2$O$_2$. The electrochemical property was investigated by cyclic voltammogram (CV) methods using the
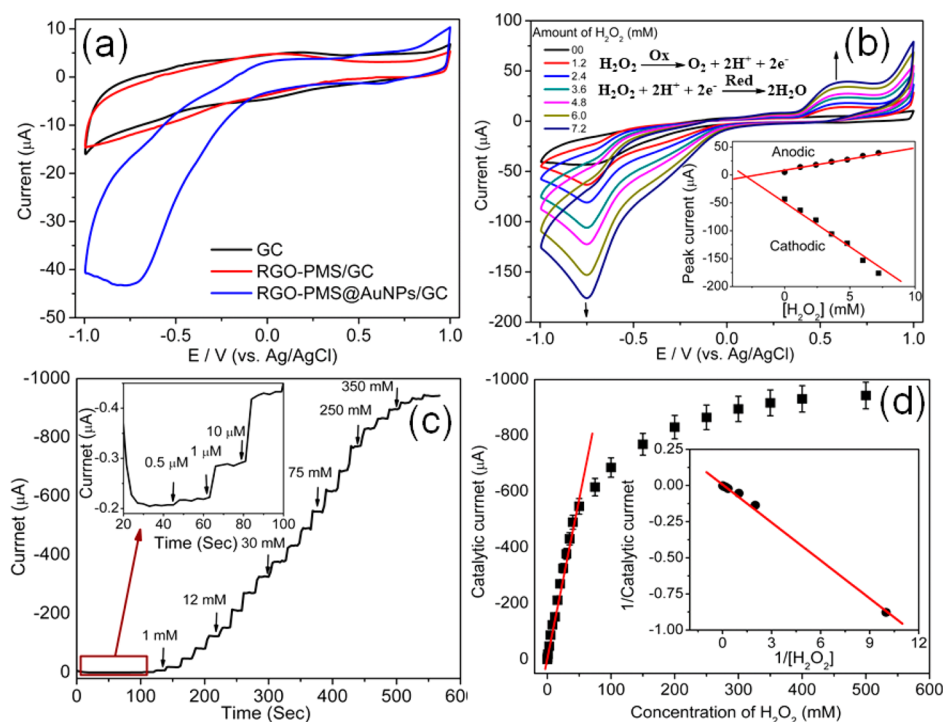
Figure 4. (a) CV curves of GC, RGO-PMS/GC, and RGO-PMS@AuNPs/GC electrodes in 0.1 M PBS. (b) CV curves of RGO-PMS@AuNPs/GC electrode in the absence and presence of H_2O_2 (inset: corresponding calibration plots). (c) Amperometric response curve and (d) corresponding calibration plot (inset: Lineweaver−Burk plot) for RGO-PMS@AuNPs/GC electrode by the successive addition of H_2O_2 into 0.1 M PBS at −0.75 V.

three-electrode cell setup in 0.1 M PBS (pH 7.4, 30 °C). The CV curves were measured in the potential range of −1.0 to 1.0 V to identify the oxidation and reduction peak potentials of RGO-PMS@AuNPs/GC electrode for electrochemical sensing of H_2O_2. Figure 4a shows the typical CV curves of bare GC, RGO-PMS/GC, and RGO-PMS@AuNPs/GC electrodes, in which a substantial enhancement in the current signal with a reduction peak potential at −0.75 V was observed for the RGO-PMS@AuNPs/GC electrode under an optimized condition (see Figure S5 in the Supporting Information for pH and temperature optimization), indicating its excellent electrocatalytic property. It was also observed from EIS (Supporting Information Figure S6) that the charge transfer resistance was significantly reduced from 522.09 to 125.0 Ω for the RGO-PMS@AuNPs/GC electrode as compared to bare GC electrode, demonstrating the superior electron transfer capability of the hybrid material.

The electrochemical sensing behavior to H_2O_2 was studied under the standardized cell setup conditions. As shown in Figure 4b, after the addition of H_2O_2 to PBS, the current signal increased significantly with the appearance of well-defined cathodic and anodic peaks at −0.75 and +0.65 V corresponding to obvious reduction and oxidation of H_2O_2.[34,36] The electrochemical sensing behavior of RGO-PMS@AuNPs/GC electrode was further investigated with the successive addition of H_2O_2 (1.2−7.2 mM) to PBS. It was observed that both the cathodic and the anodic peak currents increased significantly with a linear relationship to the successive addition of H_2O_2 (inset of Figure 4b), firmly demonstrating an excellent H_2O_2 sensing capability of the constructed electrode. The typical diffusion-controlled electrochemical reaction mechanism was then established by measuring the linear increment of cathodic

and anodic peak currents at various scan rates (Supporting Information Figure S7).

The enhanced electrocatalytic activity of RGO-PMS@AuNPs/GC electrode could be ascribed to the synergistic effect of RGO, PMS, and small AuNPs. RGO-PMS provides a large specific surface area, which increases the loading capacity of small H_2O_2 molecule and glucose for greater accumulation on the hybrid. The small AuNPs are responsible for the active catalytic reduction/oxidation processes. Because of excellent electrical conductivity of RGO, it facilitates the electron transfer capability in the hybrid, thus improving the electrocatalytic activity. On the other hand, RGO-PMS also acts as a good platform for successful growth of highly dispersed AuNPs without serious aggregation, preserving their high catalytic performance.

Quantitative assessment of the H_2O_2 sensing property for the RGO-PMS@AuNPs/GC electrode was carried out by chronoamperometric (CA) technique with a fixed potential of −0.75 V. Figure 4c shows the typical steady-state current−time (i−t) response plot with continuous addition of aliquot amount of H_2O_2 into PBS. As expected, well-defined stepwise increment in the current responses was observed upon the addition of H_2O_2. The electrode sensor could achieve ∼95% in its steady-state current within 2 s, indicating very fast electron transfer rate and rapid diffusion of H_2O_2 to the electrode. The linear detection range from 0.5 μM to 50 mM (correlation coefficient = 0.99848) for the sensor was calculated from the calibration plot (i vs c), suggesting that the sensor could be applicable to detect H_2O_2 from nanomolar to several millimolar scales. It should be noted that the obtained linear detection range is much more attractive than previous reports using supported AuNPs, such as GN/AuNPs (5.0×10^{-4} to 5.0×10^{-3} mM),[40] GO/AuNP (1.0×10^{-4} to 2.3 mM),[35] and RGO/
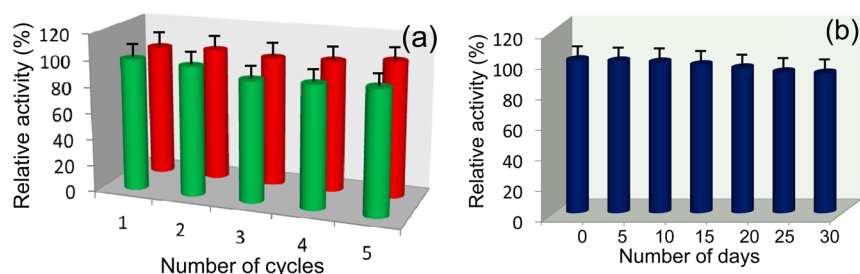
Figure 5. (a) Reproducibility (red) and stability (green) and (b) long-term storage stability (navy blue) test of the RGO-PMS@AuNPs/GC electrode measured in 0.1 M PBS.
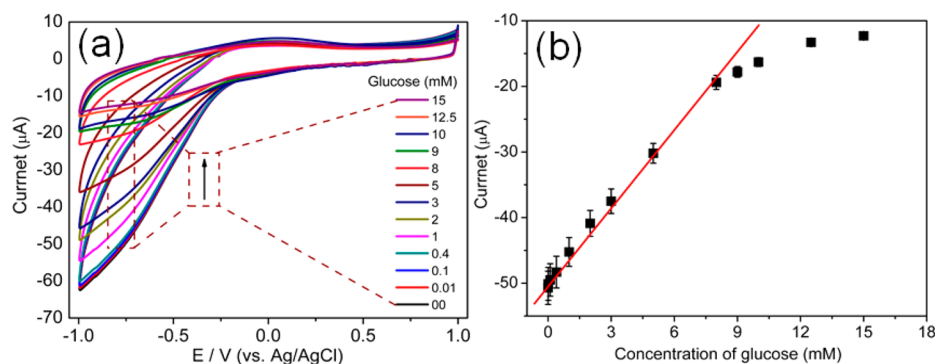

Figure 6. (a) CV curves and (b) calibration plot of RGO-PMS@AuNPs-GOD/GC electrode with successive addition of glucose to 0.1 M PBS (pH 7.4 and 30 °C).

Au paper electrodes $(1.0 \times 10^{-4}$ to 8.3 mM),[39] as well as supported PtNPs, like 3DGN/PtNPs $(1.67 \times 10^{-4}$ to 7.486×10^{-3} mM).[46] The sensitivity of the sensor was also calculated to be 39.2 μA mM^{-1} cm^{-2}, with a detection limit as low as 60 nM (S/N = 3). The obtained electrochemical parameters of the RGO-PMS@AuNPs/GC sensor are listed in Supporting Information Table S1 by comparing with some related methods reported previously. It could be clearly observed that, as compared to reported approaches, the present sensor exhibits an excellent and inherent capability for the H$_2$O$_2$ sensing in terms of wide linear detection range, low detection limit, and high sensitivity.

Because the stability and reproducibility are often required for nondisposable sensors, the stability and reproducibility of RGO-PMS@AuNPs/GC were examined to establish its application potential. As shown in Figure 5a, the same electrode retained its ∼94% activity (green bar) after five successive measurements. Moreover, the sensor showed the relative standard deviation (RSD) of ∼3.77% for five different electrodes prepared under the same technique (Figure 5a, red bar). The long-term storage stability of the sensor was also examined every 5 days up to 30 days. The same electrode was stored under dry condition at room temperature, and the relative activity versus storage days is shown in Figure 5b. After 30 days, the current-generating ability of the sensor could still be maintained at around 92% of the initial value under the same concentration of H$_2$O$_2$, indicating its good long-term stability. More importantly, the selectivity and anti-interference ability of the sensor was examined under the same response conditions of 1 mM H$_2$O$_2$ in PBS by the addition of electro-active species including uric acid (UA, 0.1 mM), ascorbic acid (AA, 0.1 mM), L-cysteine (Cys, 0.05 mM), and glutathione (GSH, 1 mM). As observed from the amperometric tests shown in Supporting Information Figure S8, no significant change in the current

signal was detected after the addition of each species under a certain time interval, suggesting the feasibility of reliable H$_2$O$_2$ determination using the developed electrode sensor in the presence of interfering species. Thus, the obtained experimental results indicate high reproducibility, stability, selectivity, and interfering resistivity of the sensor device for its future applications.

3.3. Electrochemical Sensing of Glucose and H$_2$O$_2$ in Human Urine. On the basis of the excellent performance achieved above, it was expected that the sensor could be utilized for the detection of glucose and H$_2$O$_2$ released from human urine. The glucose detection experiment was carried out using RGO-PMS@AuNPs-GOD/GC as the working electrode. Figure 6a shows the CV curves by the successive addition of glucose (0−15 mM) to PBS. The RGO-PMS@AuNPs-GOD/GC electrode exhibited a well-resolved cathodic peak at −0.75 V, which linearly decreased upon the continuous addition of glucose due to the consumption of O$_2$. The observations match well with those of the reported graphene/AuNPs/chitosan-modified GC electrode.[34] The linear range of the sensor for the detection of glucose was from 0.01 to 8 mM, calculated from the calibration plot shown in Figure 6b (correlation coefficient = 0.99802), which is applicable to the normal physiological level (3−8 mM). The sensitivity of the sensor was calculated to be 12.9 μA mM^{-1} cm^{-2}, with a low detection limit of 2.5 μM (S/N = 3). The obtained electrochemical parameters for the glucose detection are comparable to those of previously reported leading sensors summarized in Supporting Information Table S2.[34,47−49] The Michaelis−Menten constant (K_{app}^{m}) value of the developed sensor was calculated to be 3.5 mM, which is smaller than the sensors fabricated from graphene-AuNPs-GOD (4.73 mM),[50] graphene-PtNPs (5.0 mM),[51] AuNPs-PtNPs-multiwall carbon nanotubes-GOD (10.73 mM),[52] and GOx/PAni/PAN/Pt (13 mM),[48] indicating a
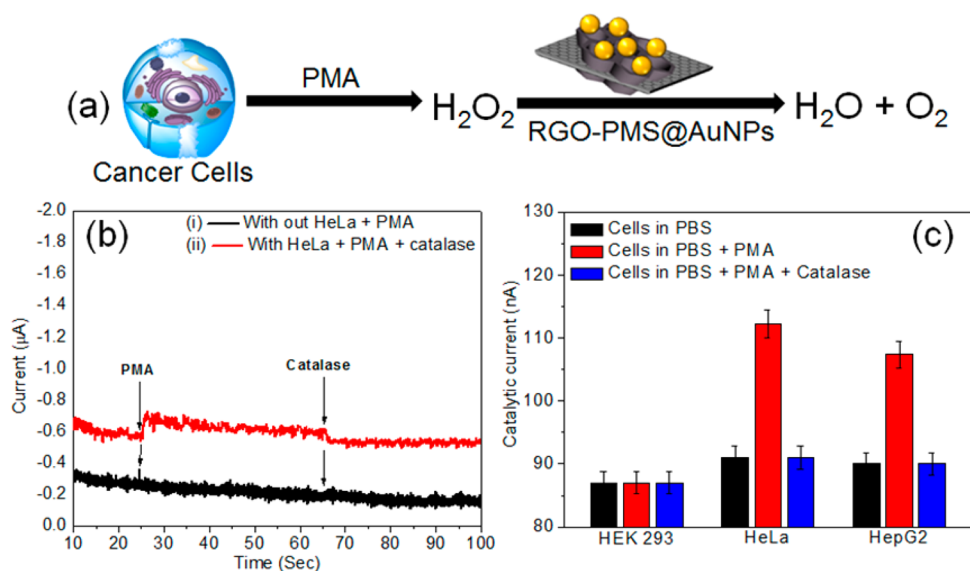
Figure 7. (a) Schematic diagram for in vitro detection of H_2O_2. (b) Amperometric response of the RGO-PMS@AuNPs/GC electrode in the (i) absence and (ii) presence of HeLa cells upon sequential additions of PMA and catalase to 0.1 M PBS at −0.75 V. (c) Comparison in cellular assay of H_2O_2 detection for HEK 293, HeLa, and HepG2 cells.

good electrocatalytic affinity of the RGO-PMS@AuNPs-GOD/GC electrode toward glucose.

It has been already established that a sufficient amount of H_2O_2 is generated through rapid superoxide-dependent autoxidation in urine upon exposure to oxygen, and thus the extent of oxidative stress in vivo could be measured by its quantification.[53] The concentration of H_2O_2 from fresh human urine was determined by measuring the current signal and then comparing it with the calibration plot obtained for H_2O_2. The determined amount of H_2O_2 from fresh human urine was 84.9 μM. The amount of H_2O_2 was also determined at 1 h after drinking coffee and was found to be 102.7 μM, which is in good agreement with a previous report.[54] Thus, the developed sensor proves its excellent ability to determine H_2O_2 in real samples.

3.4. In Vitro Cancer Cell Detection. H_2O_2 is one of the most important molecules related to many cell functions in vivo and has been recently reported as a potential marker for tumor cells.[55−57] Consequently, the developed sensor (RGO-PMS@AuNPs/GC) was also utilized for the real-time detection of H_2O_2 released from living cells including human embryonic kidney cells (HEK 293, a normal cell line), human cervical cancer cells (HeLa), and human hepatoma cancer cells (HepG2). Phobol 12-myristate-13-acetate (PMA) was employed as a stimulating agent, which can induce the H_2O_2 generation from tumor cells within a short period of time.[55] All three cell lines were separately grown and finally collected into 0.1 M PBS medium. The experiments were carried out by amperometric technique at the applied potential of −0.75 V under the same cell setup above-mentioned (Figure 7a). Before the electrochemical experiments were performed, inherent low cytotoxicity of the material was measured by standard MTT (3-(4,5-dimethylthiazol-2-yl)-2,5-diphenyltetrazolium bromide) assay (Supporting Information Figure S9).

As shown in Figure 7b, no measurable change in the current response on the RGO-PMS@AuNPs/GC electrode was observed for PBS medium upon the addition of PMA, while an obvious change in the current signal was observed for the PBS medium containing HeLa cells upon the addition of PMA. These observations well match with the previous reports.[39,55,57]

To confirm that the generation of the current signal is only due to the H_2O_2 production from the cells, a well-known H_2O_2 scavenger catalase was then added to the system. It was found that, after the injection of catalase, the increased current became decreased to its background level. Because the catalase metabolizes H_2O_2 to water and oxygen, the observation confirms the generation of H_2O_2 from the cells. The amount of H_2O_2 released from HeLa cells was determined by measuring the current change and then comparing it to the regression equation, which was found to be ∼0.8 μM. Under identical conditions, the current responses were also measured for HEK 293 and HepG2 cells, and the comparison is shown in Figure 7c. It was clearly observed that HepG2 cells also led to a notable current signal change as that of HeLa cells upon the generation of H_2O_2 by the PMA addition, whereas the normal cells did not show any obvious change. The generated H_2O_2 from cancer cells could be well detected, which was clearly distinguished from normal cell lines. Thus, it was firmly demonstrated that the constructed RGO-PMS@AuNPs/GC electrode is a sensitive and reliable probe for the detection of H_2O_2 from cancer cells.

4. CONCLUSIONS

In summary, a novel 2-D hybrid material has been developed by the AuNP immobilization on sandwich-like mesoporous silica encapsulated RGO. An electrode device as a sensor has been fabricated using the 2-D hybrid material for the electrochemical detection and quantification of H_2O_2 in aqueous medium under physiological conditions. The sensor exhibits attractive performance for sensitive and selective detection of H_2O_2 with wide linear detection range, low detection limit, and high sensitivity. The sensor has been practically applied to determine glucose and H_2O_2 in human urine. In the advanced studies, the developed sensor has been employed to selectively detect cancer cells (HeLa and HepG2) with the distinguishability from normal cells. Thus, the hybrid shows a promising application potential for biosensing and diagnostics.

ASSOCIATED CONTENT

Supporting Information

Experimental details and additional figures. This material is available free of charge via the Internet at http://pubs.acs.org.

AUTHOR INFORMATION

Corresponding Author

*E-mail: zhaoyanli@ntu.edu.sg.

Notes

The authors declare no competing financial interest.

ACKNOWLEDGMENTS

REFERENCES

(1) Yoo, S. K.; Starnes, T. W.; Deng, Q.; Huttenlocher, A. Lyn Is a Redox Sensor That Mediates Leukocyte Wound Attraction in Vivo. *Nature* **2011**, *480*, 109−112.

(2) DeYulia, G. J.; Cárcamo, J. M.; Bórquez-Ojeda, O.; Shelton, C. C.; Golde, D. W. Hydrogen Peroxide Generated Extracellularly by Receptor-Ligand Interaction Facilitates Cell Signaling. *Proc. Natl. Acad. Sci. U.S.A.* **2005**, *102*, 5044−5049.

(3) Nossol, E.; Zarbin, A. J. G. A Simple and Innovative Route to Prepare a Novel Carbon Nanotube/Prussian Blue Electrode and Its Utilization as a Highly Sensitive H_2O_2 Amperometric Sensor. *Adv. Funct. Mater.* **2009**, *19*, 3980−3986.

(4) Winterbourn, C. C. Reconciling the Chemistry and Biology of Reactive Oxygen Species. *Nat. Chem. Biol.* **2008**, *4*, 278−286.

(5) Sitnikova, N. A.; Borisova, A. V.; Komkova, M. A.; Karyakin, A. A. Superstable Advanced Hydrogen Peroxide Transducer Based on Transition Metal Hexacyanoferrates. *Anal. Chem.* **2011**, *83*, 2359−2363.

(6) Halliwell, B.; Gutteridge, J. M. C. *Free Radicals in Biology and Medicine*, 2nd ed.; Clarendon Press: Oxford, UK, 1989.

(7) Maruyama, W.; Dostert, P.; Matsubara, K.; Naoi, M. *N*-Methyl(*R*)Salsolinol Produces Hydroxyl Radicals: Involvement to Neurotoxicity. *Free Radical Biol. Med.* **1995**, *19*, 67−75.

(8) Miller, E. W.; Albers, A. E.; Pralle, A.; Isacoff, E. Y.; Chang, C. J. Boronate-Based Fluorescent Probes for Imaging Cellular Hydrogen Peroxide. *J. Am. Chem. Soc.* **2005**, *127*, 16652−16659.

(9) Rhee, S. G. H_2O_2, a Necessary Evil for Cell Signaling. *Science* **2006**, *312*, 1882−1883.

(10) Capasso, M.; Bhamrah, M. K.; Henley, T.; Boyd, R. S.; Langlais, C.; Cain, K.; Dinsdale, D.; Pulford, K.; Khan, M.; Musset, B.; Cherny, V. V.; Morgan, D.; Gascoyne, R. D.; Vigorito, E.; DeCoursey, T. E.; MacLennan, I. C. M.; Dyer, M. J. S. HVCN1Modulates BCR Signal Strength via Regulation of BCR-Dependent Generation of Reactive Oxygen Species. *Nat. Immunol.* **2010**, *11*, 265−272.

(11) Matsubara, C.; Kawamoto, N.; Takamura, K. Oxo[5,10,15,20-Tetra(4-Pyridyl)Porphyrinato]Titanium(IV): An Ultra-High Sensitivity Spectrophotometric Reagent for Hydrogen Peroxide. *Analyst* **1992**, *117*, 1781−1784.

(12) Belousov, V. V.; Fradkov, A. F.; Lukyanov, K. A.; Staroverov, D. B.; Shakhbazov, K. S.; Terskikh, A. V.; Lukyanov, S. Genetically Encoded Fluorescent Indicator for Intracellular Hydrogen Peroxide. *Nat. Methods* **2006**, *3*, 281−286.

(13) Effkemann, S.; Pinkernell, U.; Karst, U. Peroxide Analysis in Laundry Detergents Using Liquid Chromatography. *Anal. Chim. Acta* **1998**, *363*, 97−103.

(14) Srikun, D.; Albers, A. E.; Nam, C. I.; Iavarone, A. T.; Chang, C. J. Organelle-Targetable Fluorescent Probes for Imaging Hydrogen Peroxide in Living Cells via SNAP-Tag Protein Labeling. *J. Am. Chem. Soc.* **2010**, *132*, 4455−4465.

(15) Guo, S. J.; Wen, D.; Zhai, Y. M.; Dong, S. J.; Wang, E. K. Platinum Nanoparticle Ensemble-on-Graphene Hybrid Nanosheet: One-Pot, Rapid Synthesis, and Used as New Electrode Material for Electrochemical Sensing. *ACS Nano* **2010**, *4*, 3959−3968.

(16) Chen, W.; Cai, S.; Ren, Q.-Q.; Wen, W.; Zhao, Y.-D. Recent Advances in Electrochemical Sensing for Hydrogen Peroxide: A Review. *Analyst* **2012**, *137*, 49−58.

(17) Wu, P.; Cai, Z.; Chen, J.; Zhang, H.; Cai, C. Electrochemical Measurement of the Flux of Hydrogen Peroxide Releasing from RAW 264.7 Macrophage Cells Based on Enzyme-Attapulgite Clay Nano-hybrids. *Biosens. Bioelectron.* **2011**, *26*, 4012−4017.

(18) Liu, Z.; Zhao, B.; Shi, Y.; Guo, C.; Yang, H.; Li, Z. Novel Nonenzymatic Hydrogen Peroxide Sensor Based on Iron Oxide−Silver Hybrid Submicrospheres. *Talanta* **2010**, *81*, 1650−1654.

(19) Rad, A. S.; Mirabi, A.; Binaian, E.; Tayebi, H. A Review on Glucose and Hydrogen Peroxide Biosensor Based on Modified Electrode Included Silver Nanoparticles. *Int. J. Electrochem. Sci.* **2011**, *6*, 3671−3683.

(20) Chen, S.; Yuan, R.; Chai, Y.; Hu, F. Electrochemical Sensing of Hydrogen Peroxide Using Metal Nanoparticles: A Review. *Microchim. Acta* **2013**, *180*, 15−32.

(21) Woo, S.; Kim, Y.-R.; Chung, T. D.; Piao, Y.; Kim, H. Synthesis of a Graphene−Carbon Nanotube Composite and Its Electrochemical Sensing of Hydrogen Peroxide. *Electrochim. Acta* **2012**, *59*, 509−514.

(22) Tang, Y.; Allen, B. L.; Kauffman, D. R.; Star, A. Electrocatalytic Activity of Nitrogen-Doped Carbon Nanotube Cups. *J. Am. Chem. Soc.* **2009**, *131*, 13200−13201.

(23) Maji, S. K.; Dutta, A. K.; Biswas, P.; Karmakar, B.; Mondal, A.; Adhikary, B. Nanocrystalline FeS Thin Film Used as an Anode in Photo-Electrochemical Solar Cell and as Hydrogen Peroxide Sensor. *Sens. Actuators, B: Chem.* **2012**, *166−167*, 726−732.

(24) Reisert, S.; Schneider, B.; Geissler, H.; Gompel, M. V.; Wagner, P.; Schöning, M. J. Multi-Sensor Chip for the Investigation of Different Types of Metal Oxides for the Detection of H_2O_2 in the ppm Range. *Phys. Status Solidi A* **2013**, *210*, 898−904.

(25) Jia, F.; Shan, C. S.; Li, F. H.; Niu, L. Carbon Nanotube/Gold Nanoparticles/Polyethylenimine-Functionalized Ionic Liquid Thin Film Composites for Glucose Biosensing. *Biosens. Bioelectron.* **2008**, *24*, 945−950.

(26) Devadoss, A.; Han, H.; Song, T.; Kim, Y.-P.; Paik, U. Gold Nanoparticle-Composite Nanofibers for Enzymatic Electrochemical Sensing of Hydrogen Peroxide. *Analyst* **2013**, *138*, 5025−5030.

(27) Kim, G.; Lee, Y. E. K.; Xu, H.; Philbert, M. A.; Kopelman, R. K. Nanoencapsulation Method for High Selectivity Sensing of Hydrogen Peroxide inside Live Cells. *Anal. Chem.* **2010**, *82*, 2165−2169.

(28) Geim, A. K. Graphene: Status and Prospects. *Science* **2009**, *324*, 1530−1534.

(29) Yin, Z. Y.; Sun, S. Y.; Salim, T.; Wu, S. X.; Huang, X.; He, Q. Y.; Lam, Y. M.; Zhang, H. Organic Photovoltaic Devices Using Highly Flexible Reduced Graphene Oxide Films as Transparent Electrodes. *ACS Nano* **2010**, *4*, 5263−5268.

(30) Kim, H.; Lee, D.; Kim, J.; Kim, T.; Kim, W. J. Photothermally Triggered Cytosolic Drug Delivery via Endosome Disruption Using a Functionalized Reduced Graphene Oxide. *ACS Nano* **2013**, *7*, 6735−6746.

(31) Qian, J.; Wang, D.; Cai, F. H.; Xi, W.; Peng, L.; Zhu, Z. F.; He, H.; Hu, M. L.; He, S. Observation of Multiphoton-Induced Fluorescence from Graphene Oxide Nanoparticles and Applications in in-Vivo Functional Bioimaging. *Angew. Chem., Int. Ed.* **2012**, *51*, 10570−10575.

(32) Han, S.-T.; Zhou, Y.; Wang, C.; He, L.; Zhang, W.; Roy, V. A. L. Layer-by-Layer-Assembled Reduced Graphene Oxide/Gold Nano-particle Hybrid Double-Floating-Gate Structure for Low-Voltage Flexible Flash Memory. *Adv. Mater.* **2013**, *25*, 872−877.

(33) Ma, X.; Qu, Q.; Zhao, Y.; Luo, Z.; Zhao, Y.; Ng, K. W.; Zhao, Y. Graphene Oxide Wrapped Gold Nanoparticles for Intracellular Raman Imaging and Drug Delivery. *J. Mater. Chem. B* **2013**, *1*, 6495−6500.

(34) Shan, C.; Yang, H.; Han, D.; Zhang, Q.; Ivaska, A.; Niu, L. Graphene/AuNPs/Chitosan Nanocomposites Film for Glucose Biosensing. *Biosens. Bioelectron.* **2010**, *25*, 1070−1074.

(35) Zhang, B.; Cui, Y.; Chen, H.; Liu, B.; Chen, G.; Tang, D. A New Electrochemical Biosensor for Determination of Hydrogen Peroxide in Food Based on Well-Dispersive Gold Nanoparticles on Graphene Oxide. *Electroanalysis* **2011**, *23*, 1821−1829.

(36) Liu, R.; Li, S.; Yu, X.; Zhang, G.; Zhang, S.; Yao, J.; Keita, B.; Louis, N. Facile Synthesis of Au-Nanoparticle/Polyoxometalate/Graphene Tricomponent Nanohybrids: An Enzyme-Free Electrochemical Biosensor for Hydrogen Peroxide. *Small* **2012**, *8*, 1398−1406.

(37) Wang, P.; Liu, Z.-G.; Chen, X.; Meng, F.-L.; Liu, J.-H.; Huang, X.-J. UV Irradiation Synthesis of an Au−Graphene Nanocomposite with Enhanced Electrochemical Sensing Properties. *J. Mater. Chem. A* **2013**, *1*, 9189−9195.

(38) Gu, H.; Yang, Y.; Tian, J.; Shi, G. Photochemical Synthesis of Noble Metal (Ag, Pd, Au, Pt) on Graphene/ZnO Multihybrid Nanoarchitectures as Electrocatalysis for H_2O_2 Reduction. *ACS Appl. Mater. Interfaces* **2013**, *5*, 6762−6768.

(39) Xiao, F.; Song, J.; Gao, H.; Zan, X.; Xu, R.; Duan, H. Coating Graphene Paper with 2D-Assembly of Electrocatalytic Nanoparticles: A Modular Approach toward High-Performance Flexible Electrodes. *ACS Nano* **2012**, *6*, 100−110.

(40) Fang, Y.; Guo, S.; Zhu, C.; Zhai, Y.; Wang, E. Self-Assembly of Cationic Polyelectrolyte-Functionalized Graphene Nanosheets and Gold Nanoparticles: A Two-Dimensional Heterostructure for Hydrogen Peroxide Sensing. *Langmuir* **2010**, *26*, 11277−11282.

(41) Wang, Z.-M.; Wang, W.; Coombs, N.; Soheilnia, N.; Ozin, G. A. Graphene Oxide Periodic Mesoporous Silica Sandwich Nanocomposites with Vertically Oriented Channels. *ACS Nano* **2010**, *4*, 7437−7450.

(42) Hummers, W. S.; Offeman, R. E. Preparation of Graphitic Oxide. *J. Am. Chem. Soc.* **1958**, *80*, 1339−1339.

(43) Shang, L.; Bian, T.; Zhang, B.; Zhang, D.; Wu, L.-Z.; Tung, C.-H.; Yin, Y.; Zhang, T. Graphene-Supported Ultrafine Metal Nanoparticles Encapsulated by Mesoporous Silica: Robust Catalysts for Oxidation and Reduction Reactions. *Angew. Chem., Int. Ed.* **2014**, *53*, 250−254.

(44) Zhu, C.; Han, L.; Hu, P.; Dong, S. In Situ Loading of Well-Dispersed Gold Nanoparticles on Two-Dimensional Graphene Oxide/SiO_2 Composite Nanosheets and their Catalytic Properties. *Nanoscale* **2012**, *4*, 1641−1646.

(45) Gu, H.; Wang, J.; Ji, Y.; Wang, Z.; Chen, W.; Xue, G. Facile and Controllable Fabrication of Gold Nanoparticles-Immobilized Hollow Silica Particles and Their High Catalytic Activity. *J. Mater. Chem. A* **2013**, *1*, 12471−12477.

(46) Cao, X.; Zeng, Z.; Shi, W.; Yep, P.; Yan, Q.; Zhang, H. Three-Dimensional Graphene Network Composites for Detection of Hydrogen Peroxide. *Small* **2013**, *9−10*, 1703−1707.

(47) Luo, D.; Wu, L.; Zhi, J. Fabrication of Boron-Doped Diamond Nanorod Forest Electrodes and Their Application in Nonenzymatic Amperometric Glucose Biosensing. *ACS Nano* **2009**, *3*, 2121−2128.

(48) Zhai, D.; Liu, B.; Shi, Y.; Pan, L.; Wang, Y.; Li, W.; Zhang, R.; Yu, G. Highly Sensitive Glucose Sensor Based on Pt Nanoparticle/Polyaniline Hydrogel Heterostructures. *ACS Nano* **2013**, *7*, 3540−3546.

(49) Chen, K.-J.; Su, W.-N.; Pan, C.-J.; Cheng, S.-Y.; Rick, J.; Wang, S.-H.; Liu, C.-C.; Chang, C.-C.; Yang, Y.-W.; Wang, C.-H.; Hwang, B.-J. Dendritic Platinum-Decorated Gold Nanoparticles for Non-Enzymatic Glucose Biosensing. *J. Mater. Chem. B* **2013**, *1*, 5925−5932.

(50) Chen, Y.; Li, Y.; Sun, D.; Tian, D.; Zhang, J.; Zhu, J.-J. Fabrication of Gold Nanoparticles on Bilayer Graphene for Glucose Electrochemical Biosensing. *J. Mater. Chem.* **2011**, *21*, 7604−7611.

(51) Dey, R. S.; Raj, C. R. Development of an Amperometric Cholesterol Biosensor Based on Graphene−Pt Nanoparticle Hybrid Material. *J. Phys. Chem. C* **2010**, *114*, 21427−21433.

(52) Chu, X.; Duan, D.; Shen, G.; Yu, R. Amperometric Glucose Biosensor Based on Electrodeposition of Platinum Nanoparticles onto Covalently Immobilized Carbon Nanotube Electrode. *Talanta* **2007**, *71*, 2040−2047.

(53) Kuge, N.; Kohzuki, M.; Sato, T. Relation between Natriuresis and Urinary Excretion of Hydrogen Peroxide. *Free Radical Res.* **1999**, *30*, 119−123.

(54) Chatterjee, S.; Chen, A. Functionalization of Carbon Bucky-paper for the Sensitive Determination of Hydrogen Peroxide in Human Urine. *Biosens. Bioelectron.* **2012**, *35*, 302−307.

(55) Wang, T.; Peng, Z.; Wang, Y.; Tang, J.; Zheng, G. MnO Nanoparticle@Mesoporous Carbon Composites Grown on Conducting Substrates Featuring High-performance Lithium-Ion Battery, Supercapacitor and Sensor. *Sci. Rep.* **2013**, *3*, 2693.

(56) Sun, X.; Guo, S.; Liu, Y.; Sun, S. Dumbbell-Like PtPd-Fe_3O_4 Nanoparticles for Enhanced Electrochemical Detection of H_2O_2. *Nano Lett.* **2012**, *12*, 4859−4863.

(57) Xiao, F.; Li, Y.; Zan, X.; Liao, K.; Xu, R.; Duan, H. Growth of Metal−Metal Oxide Nanostructures on Freestanding Graphene Paper for Flexible Biosensors. *Adv. Funct. Mater.* **2012**, *22*, 2487−2494.